Romanian Reports in Physics **72**, 506 (2020)

MICROSTRUCTURAL AND ELECTRICAL TRANSPORT PROPERTIES OF $RBa_2Cu_3O_{7-\delta}$ (R = Y, Pr) BASED THIN FILMS AND RAMP-TYPE JOSEPHSON JUNCTIONS

V. LECA[1,*], N. D. SCARISOREANU[2], M. DINESCU[2]

[1] Horia Hulubei National Institute for R&D in Physics and Nuclear Engineering, 30 Reactorului Street, 07715 Magurele, Romania
[*] Corresponding author e-mail: *victor.leca@eli-np.ro*
[2] National Institute for Lasers, Plasma and Radiation Physics, 409 Atomistilor Street, PO-Box MG-16, 077125 Magurele, Bucharest, Romania
E-mails: *nicu.scarisoreanu@inflpr.ro*, *maria.dinescu@inflpr.ro*

Received April 23, 2020

Abstract. The results of a study on the fabrication and properties of $RBa_2Cu_3O_{7-\delta}$ (R = Y, Pr) – based thin films and ramp-type Josephson junctions are presented. The films were grown on (001) $SrTiO_3$ substrates by radio frequency plasma-assisted pulsed laser deposition (PLD) or by conventional PLD and their morphological, structural, and electrical properties were analyzed. The ramp morphology and the quality of the interfaces with the barrier and the top-electrode were found to be critical factors limiting the transport of charge carrier between the superconducting electrodes of the junctions.

Key words: pulsed laser deposition, $YBa_2Cu_3O_{7-\delta}$, ramp-type junctions.

1. INTRODUCTION

Many of the superconducting devices have as active element the so-called Josephson junction, formed by two superconducting electrodes separated by a thin, non-superconducting barrier [1–5]. Development of nanotechnologies based on high critical-temperature (T_c) superconductors (HTSc) depends on knowledge of the structural and electrical transport properties of these materials, as well as on the reproducibility of the fabrication process [4, 6–9]. Some important requirements of the circuits based on HTSc Josephson junctions are the necessity to operate in a temperature range where the low-T_c superconducting devices cannot operate and the flexibility of placing the junctions anywhere on the circuit chip [4, 6, 10]. HTSc ramp-type Josephson junctions are increasingly studied for their ability to fulfill the above requirements [8–12]. However, fine tuning of the interfaces between the superconducting electrodes and the non-superconducting barrier in this type of junctions is difficult, requiring good knowledge of the deposition method, complete insights over the structural and electrical properties of the junction's components, and of the lithography process employed for ramp and junction definition [8–15].

The use of the HTSc Josephson junctions for electronic applications requires certain characteristics of the junctions, such as large I_cR_n products (> 1mV), high-critical current density (J_c) to exceed the thermal noise level, good uniformity, and reproducibility of the junctions electrical properties [11, 12]. Epitaxial multilayer junctions with an artificial barrier, such as the ramp-type junctions, are increasingly used in fabrication of devices based on HTSc materials due to their promising electrical properties [9, 13]. For example, the ramp-type junctions based on *c*-axis oriented $YBa_2Cu_3O_{7-\delta}$ thin films make use of the longer superconducting coherence length in the a–b plane, ξ_{ab}, of about 15–20 Å, as compared with the *c*-axis coherence length, ξ_c, of about 3 Å, giving more flexibility in the junction barrier thickness [10–12, 16]. However, for practical applications of this type of junctions a better knowledge of their electrical properties' dependence on the films and ramps characteristics is still required.

In this paper we present the results on the fabrication process and characterization of $RBa_2Cu_3O_{7-\delta}$ (RBCO, R = Y, Pr) thin films and YBCO/PBCO/YBCO Josephson junctions, in the ramp-type configuration, with focus on the role of the films microstructure and of the substrate-top electrode interface on the electrical transport properties of the junctions. PBCO was selected as the barrier material being isostructural with YBCO, the junctions using this material as barrier layer having a lower junction capacitance determined by the overlap area, as compared with the case of $SrTiO_3$ (due to its large permittivity, ε), for example [10]. Also, due to its high electrical resistivity, similar thermal extension coefficient, and similar deposition parameters with the YBCO electrodes, PBCO is one of the most used barrier material for this type of junctions [10, 17]. YBCO/PBCO/YBCO ramp-type junctions with low capacitance and sufficiently large R_n, while difficult to fabricate, have potential for applications in high-frequency circuits, this being the final aim for these studies.

2. EXPERIMENTAL PROCEDURE

For revealing the surface morphology features of the samples, an XE-100 Park Systems instrument was used for atomic force microscopy (AFM) studies in contact mode (in air), with standard Si_3N_4 triangular contact mode tips ($k = 0.58$ Nm^{-1}), keeping the total interaction force as low as possible. In order to reduce the contamination of the surface, that would affect the quality of the image, the AFM scans were acquired as soon as possible after the surface treatments, for substrates, or after the deposition process, for films. For microstructural studies X-ray diffraction (XRD) scans were performed on a four-circle Rigaku Smartlab single-crystal diffractometer with rotating anode, using Cu Kα radiation. The lattice parameters of the films have been calculated from $2\theta/\omega$ scans around a series of (*hkl*) diffraction planes, all the films being considered epitaxially grown. Low incidence angle reflectivity measurements were performed as well in order to determine the film's thickness. For high-resolution transmission electron microscopy (HRTEM)

studies a Tecnai TM G2 F30 S-TWIN microscope equipped with STEM/HAADF detector, energy dispersive X-ray spectroscopy, and EFTEM-electron energy-loss spectroscopy was used, at an acceleration voltage of 300 kV obtained from a Shottky field emitter, giving a point resolution of 2 Å and a line resolution of 1.02 Å. Electrical properties were measured resistively or inductively (in order to avoid contact to the films surface, for wiring) in a cryostat with liquid N_2, down to 77 K, or with liquid He, down to 10 K.

3. RESULTS AND DISCUSSIONS

3.1. GROWTH AND PROPERTIES OF $RBa_2Cu_3O_{7-\delta}$ THIN FILMS

Before junction's fabrication, RBCO (R = Y, Pr) thin films with thickness of 50–150 nm were grown by radio-frequency (RF)-assisted PLD or by conventional PLD on (001)-oriented $SrTiO_3$ (STO) single crystal substrates, with dimensions of $10 \times 10 \times 1$ mm^3, in order to determine their morphological, structural, and electrical transport properties. A PLD setup using an ArF excimer laser (λ = 193 nm, pulsed duration 20 ns) was used for deposition, the growth conditions for the RBCO thin films being listed in Table 1. During deposition the laser beam, focused on the target using an optical system, scans horizontally the rotating target for uniform ablation. For RF-assisted PLD a 13.56 MHz radiofrequency generated oxygen plasma source was used in order to increase the reactivity of the gas species for stoichiometric and structural film's properties enhancement [18, 19]. The main advantage resulting from the use of radiofrequency discharge is related with the enhanced reactivity at the substrate or film surface (during growth) between the ablated species and the ionized and excited oxygen species coming from the plasma beam. Therefore, formation of oxygen vacancies at the substrate-film interface and/or oxygen deficiency in the films is prevented or drastically reduced. The RF-assisted PLD method has also the advantage of increasing phase stability of complex oxides for lower deposition temperatures, as well as reducing the oxygen gradient with increased film thickness [19].

Table 1

Deposition parameters for $YBa_2Cu_3O_{7-\delta}$ (YBCO) and $PrBa_2Cu_3O_{7-\delta}$ (PBCO) thin films grown by means of RF-assisted PLD or conventional PLD on (001) $SrTiO_3$ substrates

Target composition	Polycrystalline, sintered YBCO or PBCO
Substrate	(001) $SrTiO_3$, $5 \times 5 \times 1$ mm^3 size
Deposition temperature (T_d)	730–800°C
Deposition pressure (P_d)	$(18–25) \times 10^{-2}$ mbar
Laser repetition rate (f)	3–5 Hz
Deposition gas	O_2
Distance target-substrate (d_{ts})	50–65 mm
Energy density at target (E_d)	1.30–2.50 J/cm^2
RF power	150 W

All RF-assisted PLD grown YBCO films were deposited at 730°C, 0.25 mbar O_2, and an RF power of 150 W. Prior to films' deposition, each STO wafer was cleaned in organic solvents (acetone and ethanol) and then thermally treated. The thermal treatment, done at temperatures of 900–1000°C under an O_2 flow of 300 sccm, was used in order to obtain substrates with a SrO termination [20, 21], which favors a BaO termination surface of the RBCO films, thus avoiding formation of CuO_x precipitates on the films surface [22–26]. For deposition, the substrates are mounted on the heater using Ag paste allowing for good thermal contact, the substrate temperature being measured with a thermocouple. After deposition the PLD chamber was flooded with oxygen up to a pressure of about 900 mbar, at the deposition temperature. A two steps annealing procedure was then used during cooling down of the films, after flooding the chamber: the films were first annealed for 15 min at 650°C, followed by 1 h annealing at 450°C, and then cool down to room temperature. A speed of 25°C/min was used during all these steps of the cooling down procedure. The first annealing step aims to partially relax the epitaxial strain due to the mismatch between the in-plane cell parameters of the STO substrate and of the RBCO films. The second annealing step is required in order to yield superconductivity in the YBCO films by oxidation, leading to the phase transition from the tetragonal, non-superconducting structure of the as-deposited films, to the orthorhombic, superconducting structure of the oxidized films. For PBCO films the second annealing step is also required, for better oxidation. After deposition, AFM, XRD and electrical transport measurements were performed on the films.

The morphological and structural properties of the RBCO thin films were strongly dependent on the deposition parameters, such as deposition temperature (T_d), deposition pressure (P_d), substrate-target distance (d_{ts}), and the laser energy density on the target (fluence, E_d), as well as on the post-deposition annealing conditions (oxygen pressure, annealing temperature and time), which determined the oxygen composition and the crystallinity of the films. One of the critical aspects for the fabrication of the ramp-type junctions is the presence of droplets on the surface of the films, leading to pinholes *via* the barriers. To minimize the number of droplets a high-density target was used that was fine polished before each deposition, for yielding a fresh target's surface. In this way, the possibility of removing non-stoichiometric material formed during previous ablation was avoided. Deposition parameters (*i.e.*, the distance target-substrate, laser fluence) were also optimized in order to reduce the number of droplets. In Fig. 1 are shown SEM micrographs of two YBCO films grown under different deposition conditions, indicative of the role of the growth parameters on the films surface characteristics. The film from Fig. 1a was deposited at a target-substrate distance d_{ts} = 56 mm and a laser energy density on the target (fluence) of E_l = 1.75 mJ/cm^2, while the film from Fig. 1b was deposited at d_{ts} = 65 mm and E_l = 1.30 mJ/cm^2. Both films were grown at 780°C, 0.23 mbar O_2 and cooled down under 0.9 bar O_2 and annealed 1 h at 450°C. The presence of droplets is observed for the film from Fig. 1a, while only a reduced number of very small droplets can be observed in the latter case.

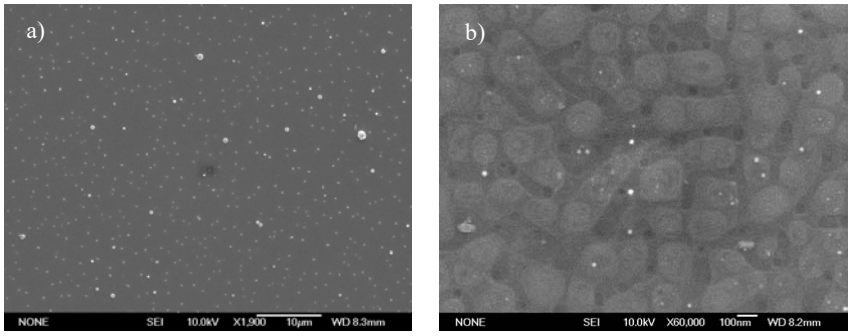

Fig. 1 – SEM micrographs (different scale) of YBCO films deposited by conventional PLD from the same target, but at different deposition parameters (see text) showing: a) the presence of large droplets, b) a reduced number of very small droplets.

Regarding the films' microstructure, the XRD data showed that the RBCO films are epitaxially grown, *c*-axis oriented. However, in some PLD grown YBCO films the presence of a-axis YBCO was also observed, although in small amount. This was the case for films grown at temperatures lower than 730°C. By increasing the deposition temperature and/or the energy of the adatoms (higher E_d) this problem could be avoided. All PLD-grown YBCO films deposited at 750–800°C were single phase, *c*-axis oriented, as well as the films grown by RF-assisted PLD (even for T_d as low as 730°C). In Fig. 2 typical 2θ/ω XRD patterns for single phase RBCO thin films epitaxially grown on (001) STO by RF-assisted PLD (Fig. 2a) and by conventional PLD (Fig. 2b and c, for YBCO and PBCO, respectively) are shown, where only reflections coming from the (00l) planes can be observed. Values for full width at half maximum (FWHM) of $\Delta\omega = 0.1–0.2°$ for (005) reflection were measured for the PLD grown YBCO and PBCO films from omega scans (rocking curves), indicating highly crystalline films. The RF-assisted YBCO films showed a larger FWHM, of about 0.25–0.55°, an indication of higher mozaicity, higher strain level, and/or smaller crystallite size. The XRD data showed that the PLD-grown YBCO films have an orthorhombic symmetry with in-plane cell parameters of $a \sim 3.835$ Å and $b \sim 3.885$ Å, while the c axis value was found to be $c \sim 11.685$ Å, with slightly larger *c*-axis value of $c \sim 11.695$ Å for the RF-assisted YBCO films. For the PBCO films the cell parameters were found to be $a \sim b \sim 3.895$ Å, and $c \sim 11.675$ Å.

The AFM analysis of the PBCO and YBCO films (Fig. 3) showed a predominantly 3D (islands) growth mode, with formation of large 3D islands, characteristic for these materials [13, 22–27]. A surface with an increased roughness resulted for the RF-assisted PLD grow films, as compared with the films grown by conventional PLD, as can be observed from the AFM images of two YBCO films shown in Fig. 3, with rms (root mean square) value of ~ 19 nm for former film (Fig. 3a), and of ~ 2 nm for latter (Fig. 3b). The PLD-grown PBCO films (Fig. 3c) showed a smoother surface compared with YBCO films and, as a

result, the surface morphology of the YBCO/PBCO bi-layers showed improvement after deposition of the PBCO layer.

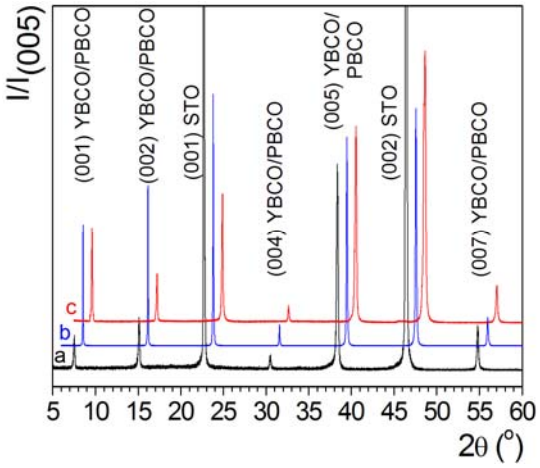

Fig. 2 – XRD 2θ/ω spectra of $YBa_2Cu_3O_{7-\delta}$ (a and b) and $PrBa_2Cu_3O_{7-\delta}$ (c) thin films grown on (001) $SrTiO_3$ substrates by RF-assisted PLD (a) and conventional PLD (b and c). Spectra (b) and (c) are shifted to the right for clarity by 1°, and by 2°, respectively. The RF-assisted PLD-$YBa_2Cu_3O_{7-\delta}$ film was grown at 0.25 mbar O_2 and 730°C, the PLD-$YBa_2Cu_3O_{7-\delta}$ film was grown at 0.25 mbar O_2 and 800°C, while the $PrBa_2Cu_3O_{7-\delta}$ film was grown at 0.18 mbar O_2 and 780°C.

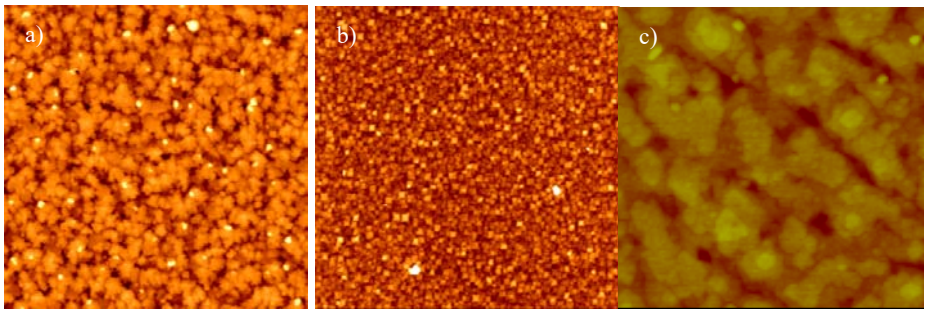

Fig. 3 – Topographic AFM images of RBCO thin films: a) YBCO grown by RF-assisted PLD (rms = 19.3 nm), b) YBCO grown by conventional PLD (rms = 2.4 nm), and c) PBCO grown by conventional PLD (rms = 1.8 nm). Scans size: 10 × 10 μm^2, for a) and b); 1 × 1 μm^2, for c).

The electrical transport measurements showed that for optimized growth conditions the YBCO thin films were superconducting, with T_c values of 85–90K, while the PBCO films showed a semiconducting like behaviour. The highest T_c values were obtained for YBCO films grown at temperatures of 780–800°C or when deposited by RF-assisted PLD, T_c value decreasing with decreasing deposition temperature. The slightly higher T_c values for the films grown using the RF plasma might be explained by a better oxygenation of the films (helped also by higher

concentration of defects in these films) and a better oxygen distribution within film thickness, characteristics of this technique [18, 19]. The morphology of the substrate surface was also found to have an influence on the electrical transport properties, a rough, untreated STO surface resulting in YBCO films with reduced T_c values, mainly due to cation off-stoichiometry [28].

3.2. FABRICATION AND PROPERTIES OF THE $YBa_2Cu_3O_{7-\delta}/PrBa_2Cu_3O_{7-\delta}/YBa_2Cu_3O_{7-\delta}$ RAMP-TYPE JUNCTIONS

A schematic representation of the YBCO/PBCO/YBCO ramp-type junctions discussed in this paper is given in Fig. 4. The use of PBCO as barrier layer is motivated by the expected low carrier scattering at the interfaces between the superconducting electrodes and the barrier [17], due to their similar crystal structure, thermal expansion coefficient, and growth conditions [10, 17]. The fabrication process of this type of junctions consisted of several steps. First, a bi-layer of 100–125 nm YBCO and 100–125 nm PBCO was deposited on an edge aligned single crystal (001) STO substrate (edge aligned – the (100) plane of the STO is aligned parallel with one of the substrate edges). All YBCO and PBCO films used in the junction's fabrication process were grown by conventional PLD due to their better microstructural and morphological properties as compared to the films grown by RF-assisted PLD. Within this bi-layer, YBCO represents the bottom electrode of the junction, while the PBCO layer represents the insulating barrier, in the *c*-axis direction, between the junction's electrodes (no current should flow in this direction between the electrodes). A positive photo resist mask is afterwards used in order to define the ramp (characterized by an angle α, see Fig. 4) by Kaufmann Ar-ion milling, the bi-layer being patterned simultaneously with the ramp. During the milling process the sample was rotated around its normal in order to yield ramps with similar angle and height, independent on their position on the substrate, and to avoid formation of kinks on the edge of the ramps due to the shadowing effect of the photoresist mask. The angle of the ramps is kept low in order to allow for epitaxial growth of the barrier and top electrode, and to avoid formation of grain boundaries at the edge of the ramps [29]. After ion milling the ramp, the photoresist was removed with acetone and ethanol.

During the ion milling process the ramp surface is damaged, resulting in off-stoichiometry, negatively affecting the junctions parameters (interface transparency, microstructure, electrical transport properties) [8–12, 30]. Following the ramp definition and removal of the photoresist, in order to reduce the damage on the ramp area, a short Ar-ion milling step with lower Ar-ions energy is used to soft clean the ramp area. In order to recrystallize the ramp area an *in-situ* annealing step is introduced before depositing the thin PBCO barrier layer. The annealing is done for 30 minutes at the deposition conditions (temperature and pressure) for YBCO. However, the annealing process does not restore the stoichiometry of the damaged area, and a region with a thickness of up to 4 nm on the ramp area surface may

have different electrical properties than of the bottom YBCO electrode and, therefore, it acts as a very thin barrier [14, 17, 31]. This barrier was shown to result in junctions with incomplete magnetic-field response due to the presence of shorts between the junction's electrodes *via* the barrier [10–14]. Therefore, after the annealing step an extra 10–25 nm thick PBCO layer was deposited, that will define the barrier in the *ab* plane of the junction. The top YBCO electrode with a thickness of 100–125 nm is afterwards deposited using the same growth parameters as for the bottom one. The junction's dimensions are then defined by optical lithography and Ar-ion milling, the excess material on top of the bottom electrode being also removed in this step, the length of the overlap area of the electrodes in the junction region being kept as small as possible (at about 3 μm) in order to reduce the junction capacitance. Finally, a 50 nm thick Au layer that will provide the electrical contacts with the junction's electrodes was DC-sputtered and then patterned. The current-voltage (*I–V)* characteristics of the junctions were then measured in liquid N_2 or in liquid He. Junctions with widths between 5 and 50 μm were placed on the same chip, with the ramp area parallel to the [100] or [110] crystallographic directions of the substrate. A SEM micrograph of a 50 μm wide ramp-type junction positioned parallel to the [110]-STO is shown in Fig. 5, where the junction components are indicated. The junction was fabricated with 100 nm thick YBCO electrodes, separated in the *c*-axis direction by a 120 nm thick PBCO insulating layer, and by ~20 nm thick PBCO barrier.

The shape and morphology of the ramps were investigated by AFM, Fig. 6 showing the morphology on the ramp area of an YBCO/PBCO bi-layer. A smooth surface of the ramp area and lack of redeposited material on the ramp edge can be observed; however, some "spikes" appear on the ramp edge that may act as pin-holes through the barrier of the final junction. The profile of the ramps was determined mainly by the shape of the edge of the photoresist mask, and less by the milling angle (the angle between the ion beam and the surface normal). In order to obtain a ramp with an angle of $15 \pm 5°$, the photoresist mask was post-baked at 120°C, for 5 minutes. This baking makes the photoresist to flow, producing a round shape of the mask edge. By using this type of photoresist mask the Ar-ion milling could also be done without any tilt angle (ion beam perpendicular to the sample surface), resulting in the desired ramp angle.

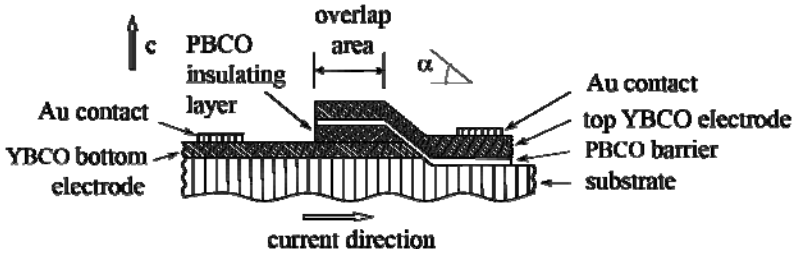

Fig. 4 – Schematic representation of the ramp-type junction.

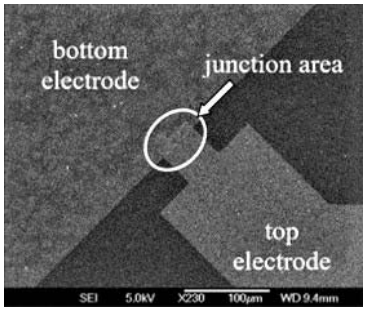

Fig. 5 – SEM micrograph of a 50 μm wide YBCO/PBCO/YBCO ramp-type Josephson junction.

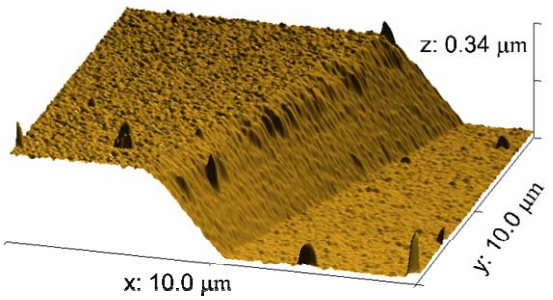

Fig. 6 – Topographic AFM image of the ramp area of an YBCO/PBCO bi-layer.

The ramp morphology and shape were found to be critical factors in observing Cooper pair tunnelling *via* the junctions, improved *I–V* characteristics being obtained for YBCO and PBCO films with reduced roughness, resulting in smooth ramps area. This is explained by the fact that the film's surface morphology is translated to the ramp area *via* the photoresist during the ion-milling process, while the ramp morphology influences the thickness distribution of the ramp barrier layer, and thus the junction's *I–V* characteristics [32, 33]. Rotation of the sample around its normal during Ar-ion milling assured that there is no re-deposited material on the edge of the ramp (as can be seen in Fig. 6), as well as a uniform distribution of the ramp angle and height for all the junctions from the same chip.

The *I–V* characteristic at 4.2 K of a 5 μm wide YBCO/PBCO/YBCO ramp-type junction with 100 nm thick top and bottom YBCO electrodes, 120 nm thick insulating PBCO layer, and 15 nm thick PBCO barrier is shown in Fig. 7. The effective coherence length of PBCO being estimated at $\xi_n \sim 5–8$ nm, for this barrier thickness the junction can be considered as junction with thick barrier [17]. The non-hysteretic *I–V* curve from Fig. 7 shows a behaviour that can be described by the resistively shunted junction (RSJ) model, the small rounding being attributed to flux flow, with flux trapping at the ramp being enhanced by the ramp structure [34]. An I_cR_n value of ~0.77 mV, for measured I_c of ~5.6 μA and R_n of ~138 Ω (estimated from the slope at high voltage), was calculated from this characteristic, at 4.2 K. The critical current density, J_c, of the junction, calculated from $J_c = I_c/A_j$, is about 200 A/cm^2 at 4.2K, with $A_j = w \cdot h/\sin\alpha$ (where A_j-junction area, w-junction width, h-thickness of the YBCO bottom electrode, α-the ramp angle, with $I_c = 5.6$ μA, $w = 5$ μm, $h = 100$ nm, and $\alpha = 15°$). The normal state resistivity $\rho_n = R_n \cdot A_j$ is calculated to be $\rho_n \sim 2.8 \cdot 10^{-6}$ Ωcm^2, with $A_j = 2 \cdot 10^{-8}$ cm^2, indication of low-ohmic weak-link structure [17]. The obtained J_c and ρ_n values are similar to those previously reported for this type of junctions [28]. The reduced I_cR_n value (if compared to the gap voltage of ~20 mV) can be explained by the interface effects and inelastic transport *via* the barrier [15]. The presence of a large excess current, I_e, can be observed for this junction in Fig. 7, an indication of electrical shorts (pin holes) between the YBCO electrodes *via* the PBCO barrier, on the ramp area.

Most of the junctions showed a resistive behaviour at temperatures higher than about 50 K. A possible reason for the temperature limitation of this type of junctions is the reduced quality of the top superconductive electrode (the electrode grown on the Ar-ion milled area of the substrate and ramp). Therefore, we have studied the electrical transport and microstructural properties of YBCO layers grown on previously Ar-milled STO substrate, as well as the microstructure of the film-substrate interface, in order to better understand the characteristics of YBCO top electrode, especially on the region that was etched during the fabrication process. Reduced T_c values of 65–70 K were measured for these YBCO layers, while HRTEM analysis (Fig. 8) indicated a high degree of structural disorder at STO-YBCO interface, findings that correlates well the limited electrical transport properties of the junctions to the degraded superconducting properties of the top electrode and of the ramp area interface with the thin barrier [35]. This adds to possible degradation of the superconducting properties of the YBCO electrodes during the lithography process, resulting in reduced working temperatures of the junctions. Also, the thin PBCO barrier layer grown on top of the Ar-milled surface of the ramp and of the substrate (as part of the junction fabrication process) is expected to contain structural disorder and off-stoichiometry [10], as HRTEM data showed, that are then transmitted to the top YBCO electrode. Optimization of the junction fabrication process, especially of the recrystallization step of the ramp area, as well as of the milled STO region, is required for obtaining junctions with improved *I*–*V* characteristics at temperatures up to 80 K, a condition for this type of junctions to be used in electronic devices [4, 6, 7, 10]. Also, fabrication of ramp-type junctions on an already ramped-substrate (previous to the deposition of the junction constituents) might help improving their electrical transport properties, as was already tentatively shown in [36].

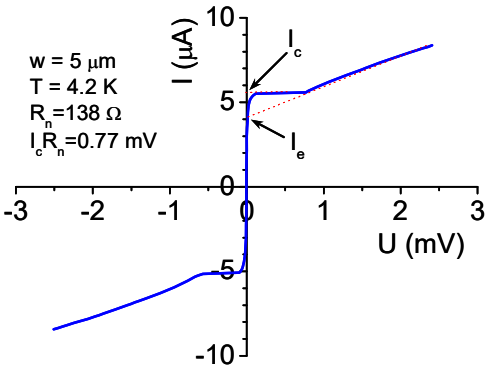

Fig. 7 – The *I*–*V* characteristic at 4.2 K of a 5 μm wide YBCO/PBCO/YBCO ramp-type junction with 100 nm thick electrodes, and 15 nm thick (ramp) barrier. The junction has a critical current I_c value of $I_c \sim 5.6$ μA.

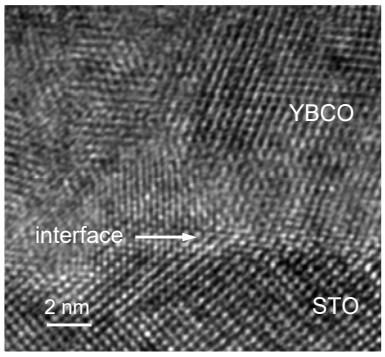

Fig. 8 – Cross section HRTEM image of part of the YBCO-STO interface region; the substrate was Ar-ion milled before the deposition of the YBCO layer.

4. CONCLUSIONS

RF-assisted PLD and conventional PLD methods have been used to grow high quality RBCO (R = Y, Pr) thin films onto (001) STO substrates for development of the technology for fabrication of YBCO/PBCO/YBCO ramp-type Josephson junctions. Deposition under optimum conditions (laser energy density, deposition temperature, and pressure) produces PLD-grown YBCO thin films with a sharp superconducting transition and relatively smooth surface, while PBCO was found to be a suitable candidate as barrier layer due to its good wetting of YBCO, similar crystalline structure and deposition conditions. The RF-assisted PLD grown YBCO films showed poor microstructural and morphological properties as compared with the conventional PLD produced samples. However, slightly higher T_c values have been measured for the RF-assisted PLD films, most probably due to better oxygenation, as a result of higher concentration of structural defects in these films. Regarding the YBCO/PBCO/YBCO ramp-type Josephson junctions, the main difficulty encountered during the fabrication process was the degradation of the microstructural and superconducting properties of the top YBCO electrode grown on a surface area that was Ar-milled during defining the ramp; this is considered to be due to the degraded microstructure and morphology of the underlaying layers and interfaces. The critical current I_c of the junctions was dependent on the ramp morphology, the observation of excess current indicating pin-holes in the PBCO barrier due to its thickness non-uniformity on the ramp area. The current-voltage characteristics of the junctions showed a behaviour that can be described by the resistively shunted junction model, I_cR_n values of about 0.77 mV being obtained. The reduced I_cR_n values can be explained by strong pair-braking effect in the barrier [17]. Improvement of the ramp characteristics, as well as of the interface between the top electrode and the previously etched substrate and layers are required in order to obtain higher I_cR_n values and higher working temperatures for this type of junctions.

Acknowledgments. V. L. acknowledges partial financial support by a grant of the Romanian National Authority for Scientific Research, CNCS-UEFISCDI, grant number PN-II-ID-PCE-2011-3-1065. Dr. Bogdan Vasile is acknowledged for performing the HRTEM analysis. We acknowledge the group of Physikalisches Institut-Experimentalphysik II and Center for Collective Quantum Phenomena in LISA$^+$, Universität Tübingen, Germany for providing us access to their research infrastructure and for many fruitful discussions and inputs during performing this work.

REFERENCES

1. B. D. Josephson, Phys. Lett. **1**, 251 (1962).
2. B. D. Josephson, Adv. Phys. **14**, 419 (1965).
3. A. Barone, *Physics and Applications of the Josephson Effect*, John Wiley and Son, 1982.
4. D. Koelle, R. Kleiner, F. Ludwig, E. Dantsker, and J. Clarke, Rev. Mod. Phys. **71**, 631 (1999).
5. J. Tomaschko, S. Scharinger, V. Leca, J. Nagel, M. Kemmler, T. Selistrovski, D. Koelle, and R. Kleiner, Phys. Rev. B **86**, 94509 (2012).

6. H. Nakane, Y. Tarutani, T. Nishino, H. Yamada, and U. Kawabe, Jpn. J. Appl. Phys. **26**, L1925 (1987).
7. J. Gao, W. A. M. Aarnink, G. J. Gerritsma, and H. Rogalla, Phys. C Supercond. **171**, 126 (1990).
8. H.-J. H. Smilde, H. Hilgenkamp, G. Rijnders, H. Rogalla, and D. H. A. Blank, Appl. Phys. Lett. **80**, 4579 (2002).
9. Ariando, D. Darminto, H.-J. H. Smilde, V. Leca, D. H. A. Blank, H. Rogalla, and H. Hilgenkamp, Phys. Rev. Lett. **94**, 167001 (2005).
10. M. A. J. Verhoeven, *High-Tc Superconducting Ramp-Type Junctions*, University of Twente, The Netherlands, 1996.
11. J. Gao, Y. Boguslavskij, B. B. G. Klopman, D. Terpstra, G. J. Gerritsma, and H. Rogalla, Appl. Phys. Lett. **59**, 2754 (1991).
12. J. Gao, Y. M. Boguslavskij, B. B. G. Klopman, D. Terpstra, R. Wijbrans, G. J. Gerritsma, and H. Rogalla, J. Appl. Phys. **72**, 575 (1992).
13. S. Scharinger, M. Turad, A. Stöhr, V. Leca, E. Goldobin, R. G. Mints, D. Koelle, and R. Kleiner, Phys. Rev. B **86**, 144531 (2012).
14. M. A. J. Verhoeven, R. Moerman, M. E. Bijlsma, A. J. H. M. Rijnders, D. H. A. Blank, G. J. Gerritsma, and H. Rogalla, Appl. Phys. Lett. **68**, 1276 (1996).
15. M. A. J. Verhoeven, G. J. Gerritsma, H. Rogalla, and A. A. Golubov, IEEE Trans. Appl. Supercond. **5**, 2095 (1995).
16. J. L. Sun and J. Gao, Phys. Rev. B **62**, 1457 (2000).
17. Y. M. Boguslavskij, J. Gao, A. J. H. M. Rijnders, D. Terpstra, G. J. Gerritsma, and H. Rogalla, IEEE Trans. Appl. Supercond. **3**, 2034 (1993).
18. F. Craciun, M. Dinescu, P. Verardi, N. Scarisoreanu, C. Galassi, and D. Piazza, Ferroelectrics **302**, 313 (2004).
19. N. Scarisoreanu, D. G. Matei, G. Dinescu, G. Epurescu, C. Ghica, L. C. Nistor, and M. Dinescu, Appl. Surf. Sci. **247**, 518 (2005).
20. V. Leca, *Heteroepitaxial Growth of Copper Oxide Superconductors by Pulsed Laser Deposition*, University of Twente. The Netherlands, 2003.
21. V. Leca, G. Rijnders, G. Koster, D. H. A. Blank, and H. Rogalla, MRS Proc. **587**, O3.6 (1999).
22. D. P. Norton, D. H. Lowndes, X.-Y. Zheng, S. Zhu, and R. J. Warmack, Phys. Rev. B **44**, 9760 (1991).
23. T. Haage, J. Zegenhagen, H.-U. Habermeier, and M. Cardona, Phys. Rev. Lett. **80**, 4225 (1998).
24. S. Bals, G. Van Tendeloo, G. Rijnders, D. H. A. Blank, V. Leca, and M. Salluzzo, Phys. C Supercond. Its Appl. **372**–**376**, 711 (2002).
25. S. Bals, G. Van Tendeloo, G. Rijnders, M. Huijben, V. Leca, and D. H. A. Blank, IEEE Trans. Appl. Supercond. **13**, 2834 (2003).
26. R. I. Chakalova, T. J. Jackson, G. Passerieux, I. P. Jones, P. Mikheenko, C. M. Muirhead, and C. N. W. Darlington, Phys. Rev. B **70**, 214504 (2004).
27. B. Dam, J. H. Rector, J. M. Huijbregtse, and R. Griessen, Phys. C Supercond. **305**, 1 (1998).
28. R. J. Cava, B. Batlogg, C. H. Chen, E. A. Rietman, S. M. Zahurak, and D. Werder, Phys. Rev. B **36**, 5719 (1987).
29. M. Schilling, IEEE Trans. Appl. Supercond. **7**, 2960 (1997).
30. H. J. H. Smilde, H. Hilgenkamp, G. J. Gerritsma, D. H. A. Blank, and H. Rogalla, Phys. C Supercond. **350**, 269 (2001).
31. K. Verbist, O. I. Lebedev, M. A. J. Verhoeven, R. Winchern, A. J. H. M. Rijnders, D. H. A. Blank, F. Tafuri, H. Bender, and G. Van Tendeloo, Supercond. Sci. Technol. **11**, 13 (1998).
32. C. Horstmann, P. Leinenbach, R. Dittmann, U. Memmert, U. Hartmann, and A. I. Braginski, IEEE Trans. Appl. Supercond. **7**, 2844 (1997).
33. J. Gao, Y. Yang, and J. L. Sun, IEEE Trans. Appl. Supercond. **9**, 3145 (1999).
34. A. Marx, K.-D. Husemann, B. Mayer, T. Nissel, R. Gross, M. A. J. Verhoeven, and G. J. Gerritsma, Appl. Phys. Lett. **64**, 241 (1994).
35. J. Gao, Y. Yang, and J. L. Sun, Appl. Phys. A **70**, 107 (2000).
36. B. Hogberg and Z. Ivanov, IEEE Trans. Appl. Supercond. **13**, 794 (2003).